ARTICLE

Cobalt Oxide Ordered Bowl-Like Array Films Prepared by Electrodeposition through Monolayer Polystyrene Sphere Template and Electrochromic Properties

X. H. Xia, J. P. Tu,* J. Zhang, J. Y. Xiang, X. L. Wang, and X. B. Zhao

State Key Laboratory of Silicon Materials and Department of Materials Science and Engineering, Zhejiang University, Hangzhou 310027, People's Republic of China

ABSTRACT In this paper, we report a facile method to produce large-area periodical bowl-like cobalt oxide (Co_3O_4) array films based on a self-assembled monolayer polystyrene sphere template and electrodeposition. After the template is removed, the resulting Co_3O_4 films consist of periodic, interconnected networks of monodisperse submicrometer pores with a diameter of 1 μm. Moreover, the individual bowl contains a large number of pores with a diameter of 50 $\pm$ 20 nm and the interstices between bowls are filled with Co_3O_4 nanoflakes. As a preliminary test, the electrochromic properties of the Co_3O_4 macrobowl arrays have been investigated and it is found that the film annealed at lower temperature exhibits better electrochromic performance. The Co_3O_4 array film annealed at 200 °C exhibits good electrochromism with color changes from dark gray to pale yellow and fast response times. The coloration efficiency is calculated to be 29 $cm^2\ C^{-1}$ at 633 nm, with a variation of transmittance up to 33%.

KEYWORDS: cobalt oxide • polystyrene sphere template • electrodeposition • ordered macroporous array • electrochromism

1. INTRODUCTION

Two-dimensionally (2D) ordered macroporous arrays have been the subject of extensive research in the context of material science due to their distinctive structural features and intriguing properties (1, 2). Introduction of porosity on a two-length scale in an ordered fashion with interconnectivity between the pores and the hierarchical structure would be important for the design of photonic crystals, sensors, power sources, catalysts, and various other applications (3, 4). Meanwhile, in nearly every case, the utility of the ordered porous systems is proved to be a sensitive function of the pore diameters, their distribution, and their morphology (5−7). Thus, morphology-controlled fabrication with a large area is becoming more and more important.

In the past decade, some strategies mainly based on self-assembled systems have been developed for the growth of ordered macroporous arrays. These templates include surfactants (8), biological systems (9), liquid-droplet surfaces (10), emulsions (11, 12) and monolayer colloidal crystal templates (1). Among them, colloidal monolayer lithography (typically polystyrene or silica spheres as the template) has been proven to be a promising strategy for the fabrication of various 2D ordered macroporous arrays because of its flexibility and controllable morphologies (13). The typical monolayer colloidal crystal template (MCCT) is an ordered monolayer colloidal microsphere array with a hexagonal close-packed alignment on a certain substrate (14, 15). In this approach, the interstitial spaces between colloidal spheres are infiltrated with another material and subsequent removal of the template by either wet etching or thermal decomposition leads to the formation of an ordered porous structure. Among the existing synthetic approaches of target materials infiltration into the colloidal template, electrochemical techniques have shown unique principles and flexibility in the control of the structure and morphology of macroporous arrays (16, 17). Electrochemical deposition has a number of significant advantages in this application. It gives a high density of deposited material within the voids of the template, and no shrinkage of the material occurs when the template is removed. Consequently, the resulting film is a true cast of the template structure and the size of the pores is directly determined by the size of template spheres used. Furthermore, it can be used to prepare a wide range of materials, and it also allows fine control over the thickness of the final macroporous arrays through control of the total charge passed to deposit the film.

Spinel cobalt oxide (Co_3O_4) is an important electronic and magnetic P-type semiconductor. It is classified as one of the most versatile transition-metal oxides, with applications in lithium ion batteries (18), gas sensing (19), and electrochromic devices (20). Numerous porous nanostructured Co_3O_4 materials have been synthesized and applied in different areas, while most of the research has focused on powder form materials (21−23), and there is little literature about the synthesis and application of Co_3O_4 array films. Li et al. (24) reported a mesoporous Co_3O_4 nanowire array prepared

* To whom correspondence should be addressed. Tel: (86)-571-87952573. Fax: (86)-571-87952856. E-mail: tujp@zju.edu.cn.
Received for review September 18, 2009 and accepted October 26, 2009

DOI: 10.1021/am900636g

Published on Web 11/04/2009

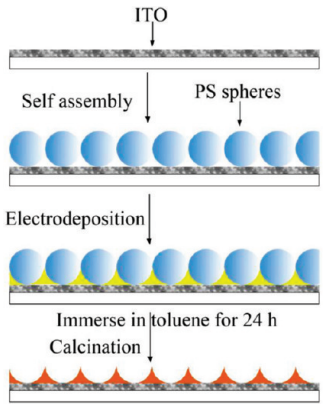

FIGURE 1. Schematic illustration for the formation of Co_3O_4 macrobowl array films.

by a templateless thermal oxidation method and its enhanced electrochemical performances for Li ion batteries. On the other hand, despite various ordered macroporous array materials, including polymers, metals, oxides, and hydroxides, have been prepared through the MCCT method (25−31), there are few reports devoted to the synthesis and application of ordered macroporous Co_3O_4 arrays. Herein, we report a facile method to controllable synthesis of ordered bowl-like Co_3O_4 arrays by the combination of electrodeposition and the MCCT method. More interestingly, the as-prepared Co_3O_4 array films have a hierarchical porous structure, in which the skeleton is composed of ordered monodisperse submicrometer pores possessing porous walls. Furthermore, as a preliminary test, their electrochromic properties are investigated. The ordered macrobowl Co_3O_4 array films are also expected to have promising applications in Li ion batteries, sensing, and field emission.

2. EXPERIMENTAL SECTION

All solvents and chemicals were of reagent quality and were used without further purification. The monodispersed PS spheres with particle sizes of 1 μm in diameter were purchased from Alfa Aesar Corp. They were well dispersed in deionized water and prepared as a suspension with concentration of 2.5 wt % before fabricating colloidal monolayers.

2.1. Assembly of a Monolayer PS Sphere Template. The fabrication process of ordered bowl-like Co_3O_4 array films involves three steps, which are schematically illustrated in Figure 1. The first step was to prepare ordered monolayer PS spheres by self-assembly. First, 5 drops of a PS suspension were dropped onto the surface of the clean indium tin oxide (ITO) substrate with a size of 1.5 × 1.5 cm^2. After the substrate was held stationary for 1 min to obtain good dispersion of the suspension, the substrate was then slowly immersed into deionized water. Once the suspension contacted the water's surface, a monolayer of PS spheres was observed to immediately form, both on the surface of the water and on the surface of the ITO substrate. To prevent any further additions to the substrate, it was kept immersed. Then, a few drops of 2% dodecyl sodium sulfate solution were added to the water to change the surface tension. As a result, the monolayer of PS spheres that remained suspended on the surface of the water was pushed aside due to the change in surface tension. Then the substrate was lifted up through the clear area, making sure that no additional PS spheres were deposited on the monolayer during this process, followed by heating at 110 °C in an oven for 5 min to bond the monolayer with the ITO substrate.

2.2. Preparation and Characterization of Ordered Bowl-like Co_3O_4 Array Films. The electrodeposition was performed in a standard three-electrode glass cell at 20 °C, with the above template electrode as working electrode, a saturated calomel electrode (SCE) as the reference electrode and Pt foil as a counter electrode. The precursor films were electrodeposited from aqueous solution containing 0.9 M $Co(NO_3)_2$ and 0.075 M $NaNO_3$ using a Chenhua Model CHI660C Electrochemical Workstation (Shanghai). The electrodeposition experiment was carried out at a constant current of 1.0 mA cm^{-2} for 300 s. The electrodeposition process of the $Co(OH)_2$ precursor film would include an electrochemical reaction, and the precipitation reaction can be expressed as (32)

$$NO_3^- + H_2O + 2e^- \rightarrow NO_2^- + 2OH^- \quad (1)$$

$$Co^{2+} + 2OH^- \rightarrow Co(OH)_2 \quad (2)$$

Afterward, the samples were immersed in toluene for 24 h to remove the PS sphere template. Finally, the as-prepared samples were dried at 85 °C and then annealed at different temperatures (200, 250, and 300 °C) in air for 1 h.

The powder from the as-deposited precursor film was analyzed by thermogravimetry (TG) and differential thermal analysis (DTA) under an N_2 atmosphere at a heating rate of 10 °C min^{-1} in the temperature range 25−520 °C. The obtained samples were characterized by X-ray diffraction (XRD) using a Rigaku D/max-ga X-ray diffractometer with graphite-monochromated Cu Kα radiation (λ = 1.541 78 Å). The images and structures of the sample were obtained by field emission scanning electron microscopy (FESEM, FEI SIRION), transmission electron microscopy (TEM, JEM 200 CX 160 kV), high-resolution transmission electron microscopy (HRTEM, JEOL JEM-2010F), and Fourier transform infrared (FTIR) measurements (Perkin-Elmer System 2000 FTIR interferometer). Atomic force microscope (AFM) images were obtained in the tapping mode on a Nanoscope IIIa Multimode scope with silicon cantilevers (NC-W, the typical frequency of 285 kHz).

2.3. Electrochromic and Electrochemical Measurements. The transmission spectra of Co_3O_4 array films in the fully colored and fully bleached states were measured ex situ over the range from 200 to 900 nm with a Shimadzu UV-2550 spectrophotometer. The electrochromic performances of the Co_3O_4 macrobowl films were measured after the films had been subjected to cyclic voltammetric tests for 30 cycles in 0.1 M KOH. The Co_3O_4 film is colored by applying a step voltage of 0.65 V for 10 s and bleached at −0.2 V (vs Hg/HgO) for 10 s. The cyclic voltammetry (CV) and chronoamperometry (CA) measurements were carried out in a three-compartment system containing 0.1 M KOH as the electrolyte, Hg/HgO as the reference electrode, and Pt foil as the counter electrode. Cyclic voltammetry (CV) measurements were performed at a scanning rate of 10 mV s^{-1} between −0.2 and 0.65 V at 25 °C.

3. RESULTS AND DISCUSSION

3.1. Synthesis and Characterization of Ordered Bowl-like Co_3O_4 Array Films. The quality of materials formed through template synthesis depends sensitively on the order and properties of the starting template. Parts a and b of Figure 2 show typical SEM images of the top and side views of the self-assembled PS sphere monolayer. In this case, the PS spheres are organized into a close-packed arrangement with long-range order both parallel and perpendicular to the ITO substrate.

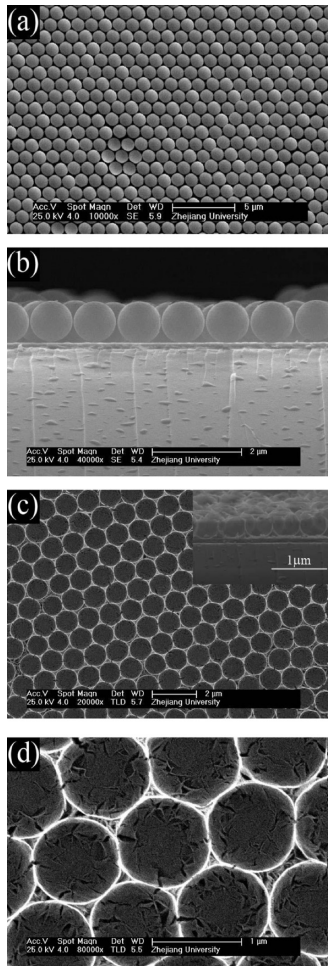

FIGURE 2. SEM micrographs of (a) top and (b) side views of the self-assembled PS sphere template and (c, d) SEM images of the Co_3O_4 macrobowl array film annealed at 200 °C for 1 h. The upper right inset in (c) corresponds to a side view of the film.

Highly ordered bowl-like arrays of Co_3O_4 are fabricated after toluene etching in combination with heat treatment (Figure 2c,d). The as-prepared Co_3O_4 films are arranged in an ordered hexagonal close-packed bowl-like array, as is usually observed in the literature (33). The skeleton of the array film is made up of macrobowls with a diameter of about 1 μm. Meanwhile, it is important to notice that the bowls contain a large number of pores with a diameter of 50 ± 20 nm and the interstices between bowls are also filled with Co_3O_4 nanoflakes (Figure 2d). Similar morphologies are observed in films annealed at 250 and 300 °C (Figure S1, Supporting Information). These pores are not the cracks resulting from the removal of the template but the interstices between Co_3O_4 nanoflakes converted from $Co(OH)_2$ ones. Previous reports have demonstrated that the $Co(OH)_2$ film electrodeposited from $Co(NO_3)_2$ exhibits a randomly porous structure composed of nanoflakes perpendicular to the substrate (32, 34). This structure is also confirmed in our experiment (see Figure S2, Supporting Information). The Co_3O_4 obtained without a PS template exhibits a highly porous structure made up of interconnected nanoflakes with a thickness of 10−25 nm (Figure S3, Supporting Information). The flakes arrange vertically to the substrate, forming a netlike structure and leaving pores of 20 −300 nm. Thus,

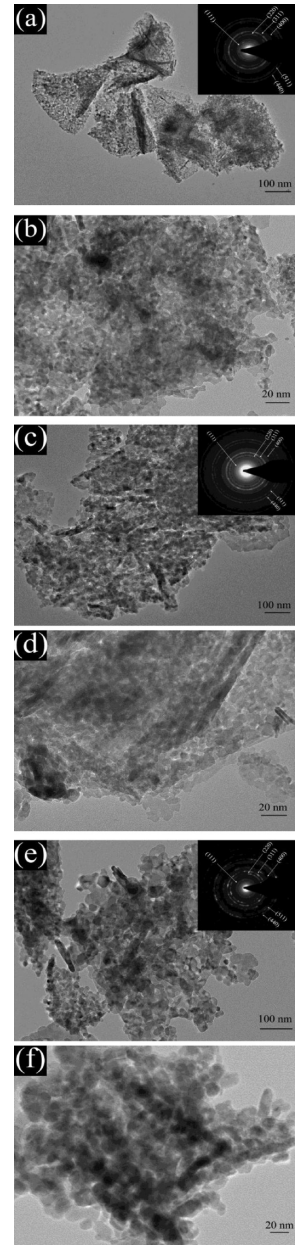

FIGURE 3. TEM images of the Co_3O_4 flakes (a, b) of film annealed at 200 °C, (c, d) of film annealed at 250 °C, and (e, f) of film annealed at 300 °C for 1 h. The upper right insets in (a), (c), and (e) correspond to the SAED patterns.

it is concluded that these bowls in the array are composed of Co_3O_4 nanoflakes perpendicular to the substrate, leaving pores of 50 ± 20 nm.

Further insight into the microstructure of the nanoflake is obtained by TEM and HRTEM. The flakes present a rough appearance composed of nanoparticles whose diameter increases as the annealing temperature increases (Figure 3). The diameters of nanoparticles for film annealed at 200, 250, and 300 °C are 4 ± 2, 7 ± 2, and 12 ± 2 nm, respectively. All the diffraction rings in the selected area electronic diffraction (SAED) pattern of the nanoflake can be indexed with the spinel Co_3O_4 phase (JCPDS 42-1467), indicating that the Co_3O_4 array is polycrystalline in nature. Furthermore, the measured lattice spacing of 0.46 nm is in

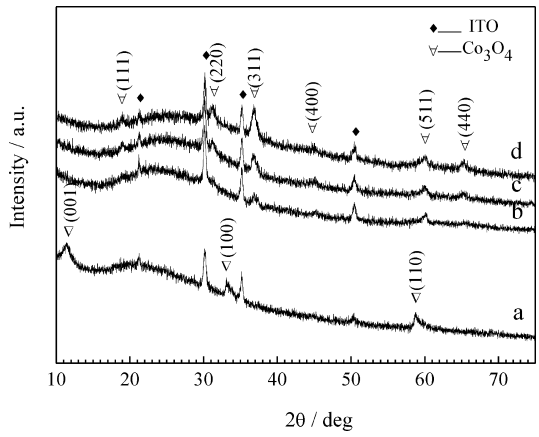

FIGURE 4. XRD patterns of (a) as-deposited precursor film and films annealed at (b) 200 °C, (c) 250 °C, and (d) 300 °C for 1 h.

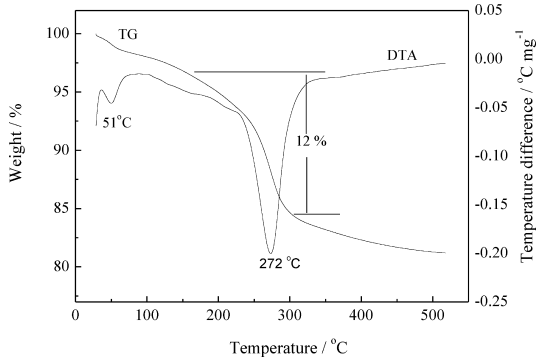

FIGURE 5. TG-DTA curves of as-deposited precursor film.

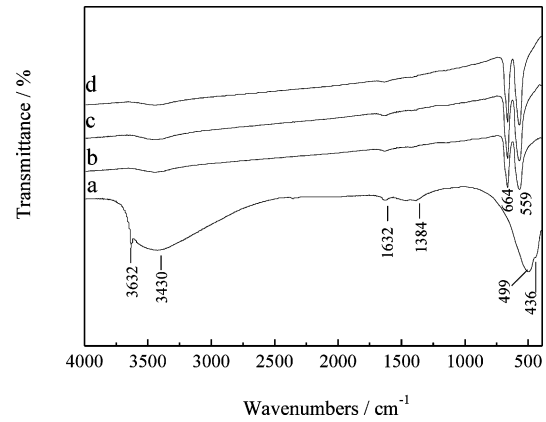

FIGURE 6. FTIR spectra of powders from (a) as-deposited precursor film and the films annealed at (b) 200, (c) 250, and (d) 300 °C for 1 h.

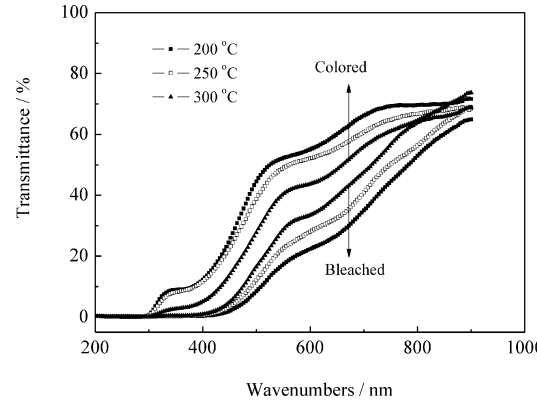

FIGURE 7. Optical transmittance spectra of Co_3O_4 array film.

good agreement with the (111) interplanar distance of the Co_3O_4 phase (Figure S4, Supporting Information).

The XRD patterns of as-deposited precursor and annealed films on ITO substrates are shown in Figure 4. The diffraction peaks of precursor films are in good agreement with the patterns of layered α-$Co(OH)_2$ (JCPDS 74-1057), similar to those reported by other authors (35). The diffraction peaks of three annealed samples can be indexed as the spinel Co_3O_4 phase (JCPDS 42-1467), indicating that the polycrystalline Co_3O_4 has formed after heat treatment, supported by the TEM results. It is also noticed that the intensities of these peaks increase with the annealing temperature, indicating that the degree of crystallinity of films increases as the annealing temperature increases.

The phase change is also confirmed by thermal analysis and FTIR. As shown in Figure 5, the main weight loss of the precursor film is in the temperature range of 150−300 °C, suggesting decomposition of cobalt hydroxide to the formation of Co_3O_4. The 12% mass loss is consistent with the expected value for a stoichiometric $Co(OH)_2$ brucite. Figure 6 shows the FTIR absorption spectra of powders from the films on ITO substrate. In the spectrum of the precursor film (Figure 6a), the peak around 3632 cm^{-1} is characteristic of non-hydrogen-bond O−H stretching vibrations of α-$Co(OH)_2$. A broad OH band centered at 3430 cm^{-1} is indicative of hydrogen-bonded water within the film structure, and the band at 1632 cm^{-1} corresponds to the angular deformation of molecular water. The peak around 1384 cm^{-1} comes from the stretching vibration of NO_3^-. The bands at 499 and 436 cm^{-1} correspond to δ(OH) and ν(CoO) vibrations, respectively. It is clearly seen from Figures 6b−d that the phase has changed after heat treatment. For the film annealed at 200 °C, the peaks in the precursor film disappear and two very strong peaks centered at 664 and 559 cm^{-1} characteristic of spinel Co_3O_4 are observed (36), indicating thorough conversion of α-$Co(OH)_2$ to Co_3O_4. For the films annealed at 250 and 300 °C, the peak intensities of Co_3O_4 increase with the annealing temperature, implying that higher annealing temperature leads to higher crystallinity.

3.2. Electrochromic Properties. The transmittance spectra of Co_3O_4 macrobowl films between the colored and bleached states are presented in Figure 7. The color of the Co_3O_4 array film changes from dark brown (colored state) to pale yellow (bleached state). Photographs of samples in the colored and bleached states are shown in Figure 8. In the annealing temperature range of 200−300 °C, the film annealed at lower temperature exhibits better optical modulation. The integrated transmittance variation (ΔT %) between the colored and bleached states for the film annealed at 200, 250, and 300 °C is 33%, 22, and 10%, respectively. The value of 33% is lower than those obtained from porous Co_3O_4 film grown by chemical bath deposition (36%) (20) and electrodeposited Co_3O_4 film (40%) (37) but much higher than those for the compact Co_3O_4 film prepared by chemical bath deposition (15%) (38) and other crystalline Co_3O_4 films

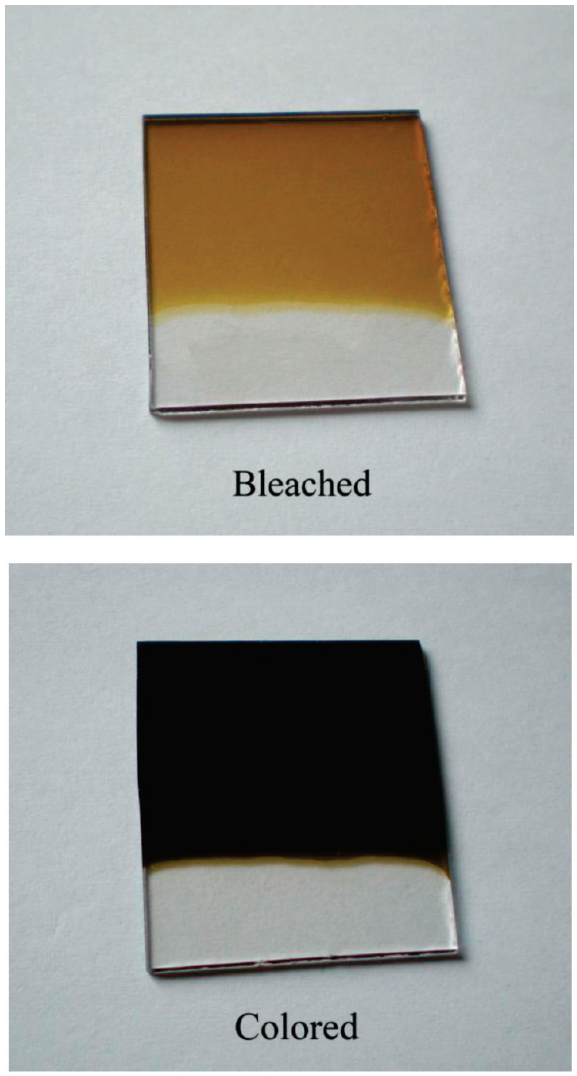

FIGURE 8. Photographs of samples with a size of 1.5 × 1.5 cm^2 in the colored and bleached states.

grown by sputtering (39), spray pyrolysis (40), and the sol−gel process (41).

The coloration efficiency (CE) is a useful figure of merit for the comparison of various electrochromic materials. CE is one of the standard methods with which to measure the effective change in optical transmission with applied potential. CE is defined as the ratio of change of optical density (ΔOD) of the film in its colored (T_c) and bleached (T_b) state at a certain wavelength and corresponding injected (or ejected) charge density (Q) per unit area. The change of optical density is obtained as

$$\eta(\lambda) = \frac{\Delta \mathrm{OD}(\lambda)}{Q} \tag{3}$$

$$\Delta \mathrm{OD}(\lambda) = \log \frac{T_b}{T_c} \tag{4}$$

The value of CE for the films annealed at 200, 250, and 300 °C is 29, 22, and 11 cm^2 C^{-1} at 633 nm, respectively.

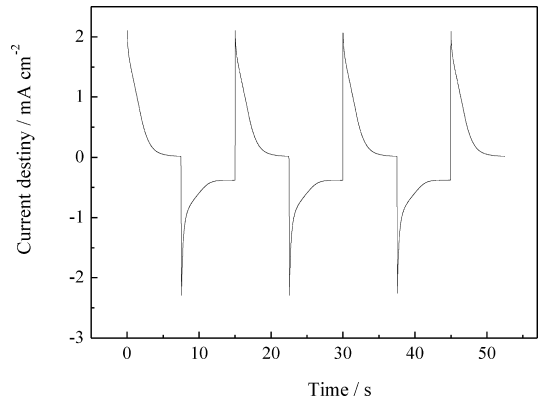

FIGURE 9. Chronoamperometric curve of the Co_3O_4 array film annealed at 200 °C for 1 h by applying alternating square potentials between 0.65 and −0.15 V (vs Hg/HgO) in 0.1 M KOH.

The value of film annealed at 200 °C is higher than those Co_3O_4 films prepared by CVD (21.5 cm^2 C^{-1}) (42), electrodeposition (20 cm^2 C^{-1}) (37), spray pyrolysis (12 cm^2 C^{-1}) (43), and the sol−gel method (25 cm^2 C^{-1}) (41).

The results above show that the annealing temperature has a great influence on the electrochromic properties of the Co_3O_4 films. The electrochromic process is actually an electrochemical process, which is associated with the double-injection (extraction) of ions and electrons to (from) the film. A higher annealing temperature is favorable to the improvement of crystalline degree, while a fully crystalline film is considered too dense for ion intercalation, resulting in low electrochromic performance. In addition, as shown in the FTIR spectra (Figure 6), the loss of free hydroxyl ion and water for a Co_3O_4 thin film annealed at higher temperature may be also responsible for the degradation of electrochromic performance (44). Therefore, an appropriate annealing temperature is at 200 °C in this work.

The response time from one state to another state is of great importance for electrochromic application. In this case, potentiostatic cycling is performed on the Co_3O_4 macrobowl array film annealed at 200 °C by applying alternating square potentials between 0.65 and −0.15 V (vs Hg/HgO). Figure 9 shows the resultant current−time response. The response times for coloration and bleaching are 4.5 and 3.5 s, respectively. This response times are slightly slower than those of randomly porous CBD Co_3O_4 film (2.5 and 2 s) (20) but faster than those of Co_3O_4 films prepared by electrodeposition (8 and 4.5 s) (37) and sol−gel (7 and 4 s) (41) and comparable to those from spray pyrolysis (4 and 2 s) (40).

In this work, the electrochromic performance of the as-prepared Co_3O_4 array film is inferior to that of randomly porous Co_3O_4 film but is superior to those grown by CVD, sol−gel, sputtering, and spray pyrolysis (37, 39−42). It is known that the electrochromic processes involve double injection (extraction) of ions and electrons into (from) the film. The processes are believed to first occur at grain boundaries and on grain surfaces. Thus, the electrochromic performance is tightly related to its morphology (45). In our previous work (20), the enhanced electrochromics of the Co_3O_4 film are mainly attributed to its highly porous struc-

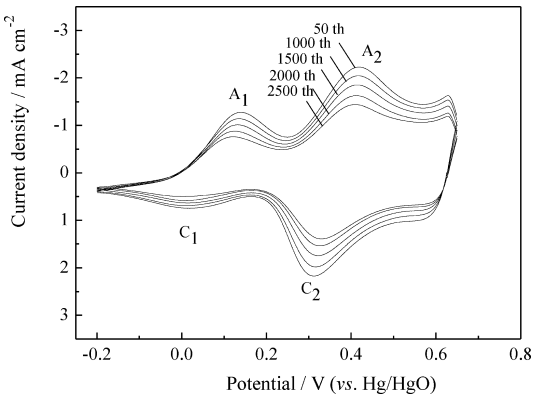

FIGURE 10. Cyclic voltammograms of the Co_3O_4 array film annealed at 200 °C for 1 h in the potential range of −0.2 to +0.65 V, at a sweep rate of 10 mV s^{-1} in 0.1 M KOH.

ture, which provides a short diffusion pathway for the counterions as well as a large active surface, leading to enhanced response time and optical modulation. In the present case, the as-prepared Co_3O_4 array films have a macroporous structure possessing less interconnected pores than the randomly porous Co_3O_4. This means that this macroporous structure provides less active area and diffusion pathway for the counterions. Even so, this macroporous film still exhibits better electrochromic properties than those compact films in the literature (37, 39−42).

The electrochemical stability of the Co_3O_4 array film annealed at 200 °C was typically characterized by cyclic voltammetry (CV) in the potential range of −0.2 to +0.65 V, at a sweep rate of 10 mV s^{-1}. The evolution of CVs is shown in Figure 10. There is a no significant change in the shape of the recorded curves. The CV curves show two typical redox peaks, which are similar to those reported by other authors (37, 46−50). The first redox couple A_1/C_1 is ascribed to the conversion between $Co(OH)_2$ (pale yellow) and Co_3O_4 (dark gray), which can be simply illustrated as (46−48)

$$3Co(OH)_2 + 2OH^- \rightarrow Co_3O_4 + 4H_2O + 2e^- \qquad (5)$$

The second redox couple corresponds to the change between Co_3O_4 and CoOOH (cobalt oxyhydroxide) (dark brown), represented by the reaction (49, 50)

$$Co_3O_4 + OH^- + H_2O \rightarrow 3CoOOH + e^- \qquad (6)$$

Upon cycling, the film switches from dark gray to pale yellow reversibly. The cycling stability of the Co_3O_4 array film in the present system has been found to be quite good. After 2500 cycles, the intensities of peak currents maintain 75% of the highest values.

4. CONCLUSIONS

In summary, we report here a facile method to fabricate large-area periodic bowl-like arrays of Co_3O_4 at room temperature by the combination of electrodeposition and a self-assembled monolayer polystyrene sphere template. It is expected that this synthetic method may be applicable to the synthesis of other macroporous electrochromic films. The as-prepared Co_3O_4 array films exhibit a hierarchical porous structure possessing pores with different sizes. The skeleton of the array film consists of macrobowls composed of nanoflakes. In addition, the Co_3O_4 array film annealed at 200 °C demonstrates good electrochromic properties, with a variation of transmittance up to 33% and a coloration efficiency of 29 cm^2 C^{-1} at 633 nm. Other applications in Li ion batteries are under investigation and will be reported in the future.

Acknowledgment. We acknowledge financial support from Zhejiang University K.P. Chao's High Technology Development Foundation (Grant No. 2008ZD001).

Supporting Information Available: SEM images of Co_3O_4 macrobowl array films annealed at 250 and 300 °C for 1 h (Figure S1), SEM images of $Co(OH)_2$ films electrodeposited without a PS template on ITO substrate (Figure S2), SEM images of Co_3O_4 films electrodeposited without a PS template on ITO substrate (Figure S3), and HRTEM images of Co_3O_4 macrobowl array films annealed at 200, 250, and 300 °C for 1 h (Figure S4). This material is available free of charge via the Internet at http://pubs.acs.org.

REFERENCES AND NOTES

(1) Yang, P.; Deng, T.; Zhao, D.; Feng, P.; Pine, D.; Chmelka, B. F.; Whitesides, G. M.; Stucky, G. D. *Science* **1998**, *282*, 2244–2246.
(2) Orilall, M. C.; Abrams, N. M.; Lee, J.; DiSalvo, F. J.; Wiesner, U. *J. Am. Chem. Soc.* **2008**, *130*, 8882.
(3) Li, Y.; Cai, W.; Duan, G. *Chem. Mater.* **2008**, *20*, 615–624.
(4) Grego, S.; Jarvis, T. W.; Stoner, B. R.; Lewis, J. S. *Langmuir* **2005**, *21*, 4971–4975.
(5) Stein, A.; Li, F.; Denny, N. R. *Chem. Mater.* **2008**, *20*, 649–666.
(6) Li, Y.; Li, C.; Cho, S. O.; Duan, G.; Cai, W. *Langmuir* **2007**, *23*, 9802–9807.
(7) Jeong, U.; Wang, Y.; Ibisate, M.; Xia, Y. *Adv. Funct. Mater.* **2005**, *15*, 1907–1921.
(8) Kresge, C. T.; Leonowicz, M. E.; Roth, W. J.; Vartuli, J. C.; Beck, J. S. *Nature* **1992**, *359*, 710–712.
(9) Davis, S. A.; Burkett, S. L.; Mendelson, N. H.; Mann, S. *Nature* **1997**, *385*, 420–423.
(10) Huck, W. T. S.; Tien, J.; Whitesides, G. M. *J. Am. Chem. Soc.* **1998**, *120*, 8267–8268.
(11) Imhof, A.; Pine, D. J. *Nature* **1997**, *389*, 948–951.
(12) Imhof, A.; Pine, D. J. *Adv. Mater.* **1998**, *10*, 697–700.
(13) Li, J.; Zhang, Y. *Chem. Mater.* **2007**, *19*, 2581–2584.
(14) Bartlett, P. N.; Baumberg, J. J.; Birkin, P. R.; Ghanem, M. A.; Netti, M. C. *Chem. Mater.* **2002**, *14*, 2199–2208.
(15) Lan, D.; Wang, Y.; Du, X.; Mei, Z.; Xue, Q.; Wang, K.; Han, X.; Zhang, Z. *Cryst. Growth Des.* **2008**, *8*, 2912–2916.
(16) Duan, G.; Cai, W.; Luo, Y.; Sun, F. *Adv. Funct. Mater.* **2007**, *17*, 644–650.
(17) Braun, P. V.; Wiltzius, P. *Nature* **1999**, *402*, 603.
(18) Idota, Y.; Kubota, T.; Matsufuji, A.; Maekawa, Y.; Miyasaka, T. *Science* **1997**, *276*, 1395–1397.
(19) Li, W.-Y.; Xu, L.-N.; Chen, J. *Adv. Funct. Mater.* **2005**, *15*, 851–857.
(20) Xia, X. H.; Tu, J. P.; Zhang, J.; Huang, X. H.; Wang, X. L.; Zhang, W. K.; Huang, H. *Electrochem. Commun.* **2008**, *10*, 1815–1818.
(21) Du, N.; Zhang, H.; Chen, B.; Wu, J. B.; Ma, X. Y.; Liu, Z.; Zhang, Y.; Yang, D. R.; Huang, X. H.; Tu, J. P. *Adv. Mater.* **2007**, *19*, 4505–4509.
(22) Lou, X. W.; Deng, D.; Lee, J. Y.; Feng, J.; Archer, L. A. *Adv. Mater.* **2008**, *20*, 258–262.
(23) Nam, K. T.; Kim, D.; Yoo, P. J.; Chiang, C.; Meethong, N.; Hammond, P. T.; Chiang, Y.; Belcher, A. M. *Science* **2006**, *312*, 885–888.

(24) Li, Y.; Tan, B.; Wu, Y. *Nano Lett.* **2008**, *8*, 265–270.
(25) Bartlett, P. N.; Birkin, P. R.; Ghanem, M. A. *Chem. Commun.* **2000**, 1671–1672.
(26) Wang, W.; Summers, C. J.; Wang, Z. L. *Nano Lett.* **2004**, *4*, 423–426.
(27) Sadakane, M.; Horiuchi, T.; Kato, N.; Takahashi, C.; Ueda, W. *Chem. Mater.* **2007**, *19*, 5779–5785.
(28) Hu, J.; Abdelsalam, M.; Bartlett, P.; Cole, R.; Sugawara, Y.; Baumberg, J.; Mahajan, S.; Denuault, G. *J. Mater. Chem.* **2009**, *19*, 3855–3858.
(29) Bartlett, P. N.; Dunford, T.; Ghanem, M. A. *J. Mater. Chem.* **2002**, *12*, 3130–3135.
(30) Fu, L. J.; Zhang, T.; Cao, Q.; Zhang, H. P.; Wu, Y. P. *Electrochem. Commun.* **2007**, *9*, 2140–2144.
(31) Fu, L. J.; Yang, L. C.; Shi, Y.; Wang, B.; Wu, Y. P. *Microporous Mesoporous Mater.* **2009**, *117*, 515–518.
(32) Zhou, W.; Zhang, J.; Xue, T.; Zhao, D.; Li, H. *J. Mater. Chem.* **2008**, *18*, 905–910.
(33) Duan, G.; Cai, W.; Luo, Y.; Li, Z.; Lei, Y. *J. Phys. Chem. B* **2006**, *110*, 15729–15733.
(34) Chou, S.; Wang, J.; Liu, H.; Dou, S. *J. Electrochem. Soc.* **2008**, *155*, A926–929.
(35) Xu, Z. P.; Zeng, H. C. *Chem. Mater.* **1999**, *11*, 67–74.
(36) Li, Y.; Tan, B.; Wu, Y. *J. Am. Chem. Soc.* **2006**, *128*, 14258–14259.
(37) Polo da Fonseca, C. N.; de Paoli, M. A.; Gorenstein, A. *Sol. Energy Mater. Sol. Cells* **1994**, *33*, 73–81.
(38) Shim, H. S.; Shinde, V. R.; Kim, H. J.; Sung, Y. E.; Kim, W. B. *Thin Solid Films* **2008**, *516*, 8573–8578.
(39) Estrada, W.; Fantini, M. C. A.; de Castro, S. C.; Polo da Fonseca, C. N.; Gorenstein, A. *J. Appl. Phys.* **1993**, *74*, 5835–5841.
(40) Patil, P. S.; Kadam, L. D.; Lokhande, C. D. *Sol. Energy Mater. Sol. Cells* **1998**, *53*, 229–234.
(41) Svegal, F.; Orel, B.; Hutchins, M. G.; Kalcher, K. *J. Electrochem. Soc.* **1996**, *143*, 1532–1539.
(42) Maruyama, T.; Arai, S. *J. Electrochem. Soc.* **1996**, *143*, 1383–1386.
(43) Kadam, L. D.; Pawar, S. H.; Patil, P. S. *Mater. Chem. Phys.* **2001**, *68*, 280–282.
(44) Xia, X. H.; Tu, J. P.; Zhang, J.; Wang, X. L.; Zhang, W. K.; Huang, H. *Sol. Energy Mater. Sol. Cells* **2008**, *92*, 628–633.
(45) Xia, X. H.; Tu, J. P.; Zhang, J.; Wang, X. L.; Zhang, W. K.; Huang, H. *Electrochim. Acta* **2008**, *53*, 5721–5724.
(46) Casella, I. G.; Gatta, M. *J. Electroanal. Chem.* **2002**, *534*, 31–38.
(47) Behl, W. K.; Toni, J. E. *J. Electroanal. Chem.* **1971**, *31*, 63.
(48) Castro, E. B.; Gervasi, C. A.; Vilche, J. R. *J. Appl. Electrochem.* **1998**, *28*, 835–841.
(49) Casella, I. G. *J. Electroanal. Chem.* **2002**, *520*, 119–125.
(50) Barbero, C.; Planes, G. A.; Miras, M. C. *Electrochem. Commun.* **2001**, *3*, 113–116.

AM900636G